Orthogonal Cutting of Gallium Nitride: A Numerical Investigation

Author

Muhammad Haseeb

Regn Number

00000277546

Supervisor

Dr. Hasan Aftab Saeed

DEPARTMENT OF MECHANICAL ENGINEERING

COLLEGE OF ELECTRICAL & MECHANICAL ENGINEERING

NATIONAL UNIVERSITY OF SCIENCES AND TECHNOLOGY

ISLAMABAD

DECEMBER, 2021

Orthogonal Cutting of Gallium Nitride: A Numerical Investigation

Author

Muhammad Haseeb

Regn Number

00000277546

A thesis submitted in partial fulfillment of the requirements for the degree of

MS Mechanical Engineering

Thesis Supervisor:

Dr. Hasan Aftab Saeed

Thesis Supervisor's Signature:_____

DEPARTMENT OF MECHANICAL ENGINEERING

COLLEGE OF ELECTRICAL & MECHANICAL ENGINEERING

NATIONAL UNIVERSITY OF SCIENCES AND TECHNOLOGY,

ISLAMABAD

DECEMBER, 2021

Declaration

It is affirmed that this thesis has been developed wholly based on my personal hard work under the immense support and valuable guidance of my supervisor Dr Hasan Aftab Saeed. Sources used are cited and contents have not been plagiarized. No part of work presented in thesis has been submitted elsewhere in any form.

………………………

Muhammad Haseeb

Language Correctness Certificate

This thesis has been read by an English expert and is free of typing, syntax, semantic, grammatical and spelling mistakes. Thesis is also according to the format given by the university.

Signature of Student

Muhammad Haseeb

Registration Number

00000277546

Signature of Supervisor

Copyright Statement

بِسْمِ اللهِ الرَّحْمٰنِ الرَّحِيْمِ

In the name of Allah, the most Beneficent and the most Merciful

Acknowledgements

Dedication

I dedicate my thesis to my family, teachers and friends. A special feeling of gratitude to my loving parents, who always believed in me and stood beside me through my thick or thin and whose words of encouragement were always there in my moral support.

I would place sincere thanks to Dr. Imran Akhtar for his guidance and support by providing all the necessary computational power required for this research work.

I pray ALLAH, for always being kind by way His countless blessings.

تو اپنی سرنوشت اب اپنے قلم سے لکھ
خالی رکھی ہے خامۂ حق نے تری جبیں

Allama Iqbal (Zarb-e-Kaleem-202)

ABSTRACT

The objective of this research is to simulate the chip formation and cutting force during the orthogonal cutting of Gallium Nitride (GaN) by conventional diamond tool. Numerical simulations were conducted to find out the Von-Mises stress, cutting force, energy balance and how these output parameters change during the machining process. The mechanical properties of GaN and Diamond, such as density, young's modulus, shear modulus, cohesion value, angle of friction, and dilation angle were taken from literature. Before conducting the numerical simulations for the machining of GaN, Steel (AISI 1045) was numerically machined, and its plastic flow stresses were matched with the published results. For Steel, Johnson-Cook material model and failure criteria were used inside ANSYS/LS-DYNA module with a rigid diamond tool. For the simulation about GaN, Mohr-Coulomb material model with Smooth Particle Hydrodynamics (SPH) approach was used. These explicit numerical simulations have been performed using ANSYS/LS-DYNA. The numerical predictions of Von-Mises stresses were found to be consistent with the literature.

Table of Contents

List of Figures

CHAPTER 1: INTRODUCTION

1.1   Background

The behavior of engineering materials can be classified into two main categories called brittle and ductile materials. Usually, ductile materials undergo large deformation before rupture whereas the plastic deformation in brittle materials is negligible. This behavior of the material depends upon the loading conditions and the operating environment for example most of them change their behavior from ductile to brittle when the temperature is lowered.
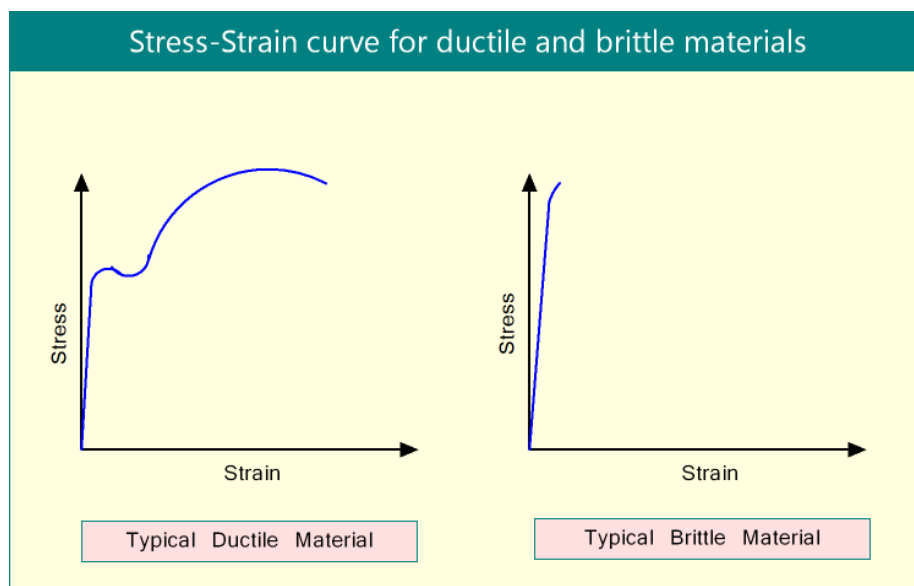
Figure 1: Stress-strain relation of ductile and brittle materials [1]

The plastic deformation is introduced when the atoms of material slide pass each other and they don't restore their original location after unloading. Most of the materials show linear response at the initial phase of loading i.e., where they follow Hooke's law and once the loading is increased

their response become nonlinear until they collapse. So, in order to machine a material, one should provide swear loading until the material ruptures or cracks in an accurate and precise manner. In order to deal with such simulations in finite element analysis, there are usually three main sources of nonlinearities to take care off. Large deformation, contact nonlinearity, and material nonlinearity. The term nonlinearity can be defined at an instance where the stiffness matrix of the system deforms with the passage of time. Material properties can be linear elastic or orthotropic. Hyper elasticity, rate and temperature dependent plasticity, pressure dependent plasticity, porosity, material strength and degradation (damage), material fracture/failure/fragmentation are some types of material nonlinearities.

1.2   Modeling and Simulation

Numerical simulations have been very useful in scientific research from previous couple of decades as they are inexpensive repeatable and safe. Generally, it starts with geometry of concern and then it is discretized according to the selected procedural approach. After discretization, appropriate material model is applied, initial and boundary conditions are set, and it is solved for the required output parameters. For Steel, workpiece selected has dimensions of 10 mm by 3 mm and it contains 34885 elements and 35421 nodes, Johnson cook material model and failure criteria are used. Workpiece is held stationary at the bottom and rigid tool is moved by giving it controlled displacement and it is solved for respective stresses, strains, contact force and energy balance. For the most concerned simulation of Gallium Nitride, Smooth Particle Hydrodynamics (SPH) approach was used while the workpiece size selected is 0.4 mm, 0.2 mm and 0.05mm. Rigid tool is moved towards the workpiece with defined displacement movement.

The reason to prefer SPH over FEM for Gallium Nitride is that SPH allows more maneuverability (can accommodate more distortion) of particles/elements than FEM, hence for machining purposes SPH is more feasible approach. The GaN simulation is solved for stresses and contact forces.

CHAPTER 2: GALLIUM NITRIDE

2.1 Background

Gallium nitride is a semiconductor which is formed when Gallium (Ga-203) reacts with Ammonia (NH_3) at high temperatures of more than 1000 degrees Celsius. It has wurtzite type structure, and it is very suitable for the electronic devices which need to tolerate swear corrosive ambient conditions.
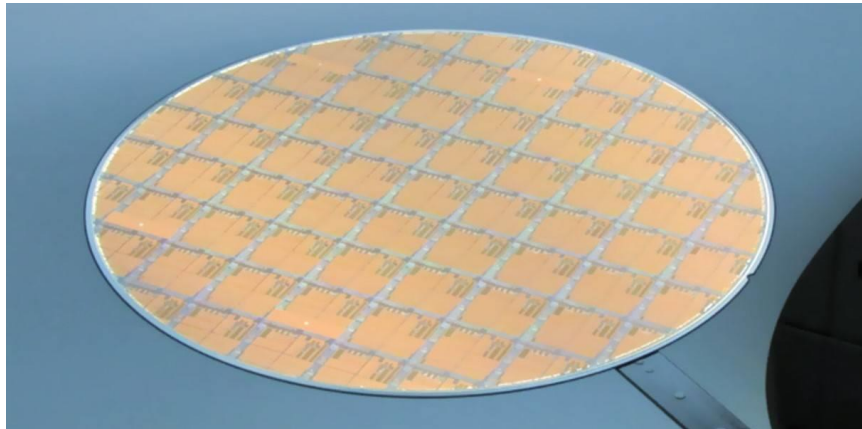
Figure 2: Gallium-Nitride wafer [2]

Its use as a semiconductor was developed in 1993 by the professors of UCSB College of Engineering, Steven den Bars, Umesh Mishra, and James Speck but later at that time due to nonavailability of research funding, it was considered useless as a semiconductor.

2.2 Significance and Advantages

Silicon has revolutionized our previous century, but its saturation point has almost been reached and most of the researchers tend to believe that Gallium Nitride (GaN) will replace the silicon in near future. GaN is an extremely useful semiconductor that has many advantages over silicon and other semiconductors. Due to its wide band gap and higher decomposition temperature, it is being used in many power applications for military, residential and commercial purposes. Military use includes radars, HEMTs (High Electron Mobility Transistors) etc., residential use includes small charging power bricks for laptops and mobile phones and commercial purposes consists of its usage in electric cars, airplanes, 5G etc.
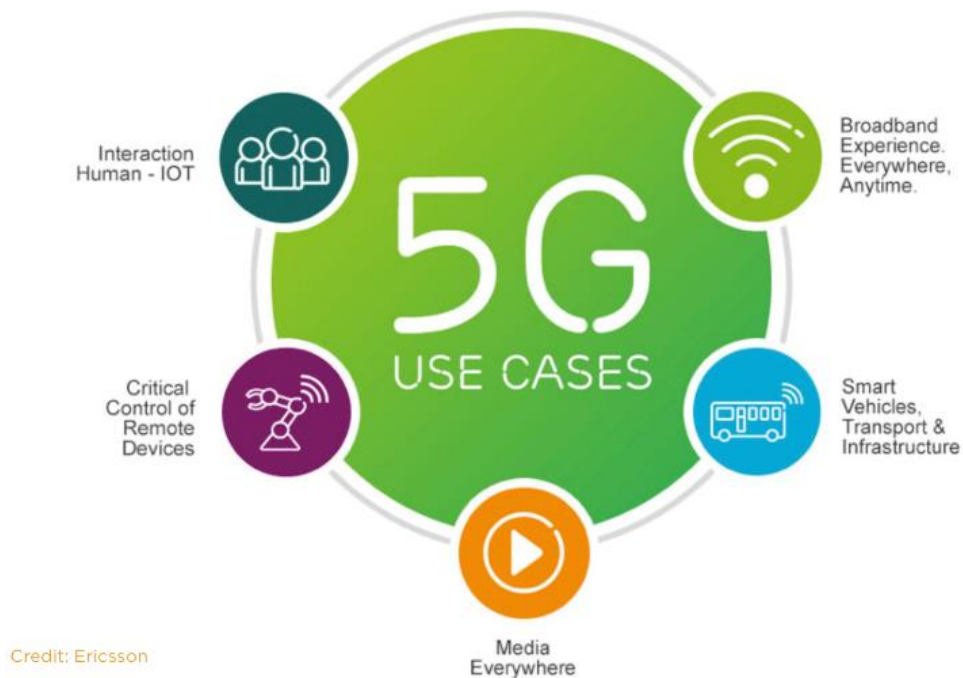
Figure 3: 5G use [3]

Figure 4: Radar system [4]
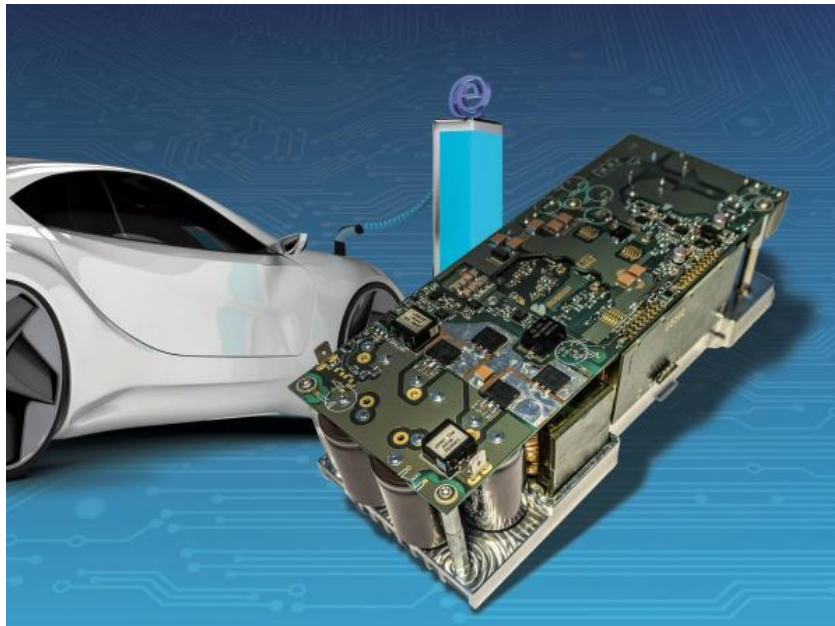
Figure 5: Compact on-board charger of 3kW uses GaN transistors [5]
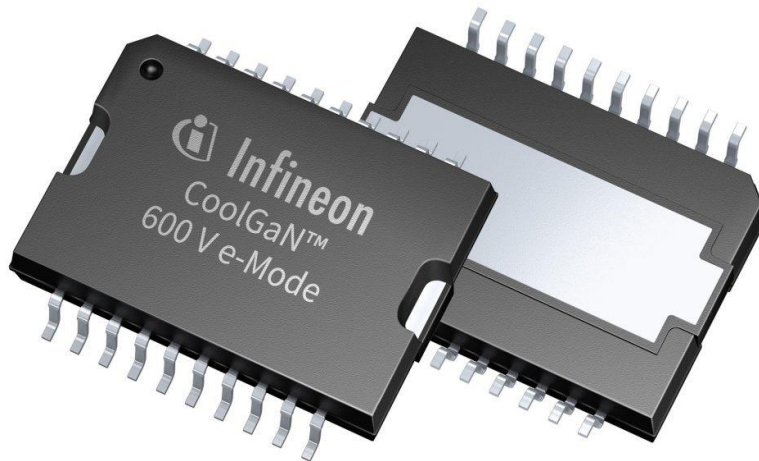
Figure 6: Gallium Nitride powered High electron mobility transistors [6]

Advantages of Gallium Nitride (GaN) over other semi-conductors are

- GaN's bandgap is three times as that of silicon

- It has very fast switching speeds, can bear high temperatures and voltages, produces less heat and thus it is preferred for power electronics applications like radars 5G and HEMTs (High Electron Mobility Transistors)

- It has higher breakdown voltage than silicon

- Much smaller chips for the same voltage can be produced by using GaN

- GaN offers less resistance to current flow and thus has less losses (around 1%).

- GaN produces higher frequency/ high power signals

- Inverters made up of GaN can make solar cells cheaper and lighter

- Entire circuitry in laptop charging brick can be replaced by a plug itself made up of GaN

- GaN can be a best candidate for upcoming quantum computing and photonics

2.3 Literature Review

Decent amount of work has already been done on the machining of Gallium Nitride, using numerical simulations and physical experimentation as well.

Gu et al. [7] machined materials like gallium nitride, sapphire and micro light emitting diodes by using Ultra-Violet (UV) copper vapor laser which was pulsed at a fixed frequency and stated that the pulsed UV vapor copper laser can easily be used for micromachining or dicing of such materials.

Kim et al. [8] studied the ablation of GaN by ultrashort pulsed laser and successfully demonstrated the controlled ablation.

Nakahama et al. [9] used plasma chemical vaporization machining (CVM) to observe the etching characteristics of GaN and reached the result that less subsurface damage is caused by plasma CVM than RIE (reactive ion etching).

Zhang et al. [10] conducted molecular dynamics simulation to investigate the mechanism of subsurface damage during nano grinding process of gallium nitride and provided an insight into low-damage processing of GaN by the subsurface damage mechanism.

Huang et al. [11] attempted to nano grind GaN using one-dimensional sinusoidal assistant vibration by molecular dynamics and found that the vibration assisted nano-grinding helped in achieving high removal rate and a surface finish of acceptable quality.

Wang et al. [12] simulated abrasive machining for wurtzite gallium nitride and explored the effect of abrasive size change on it. Reached the conclusion that increasing abrasive size increases the plastic deformation which eventually increases atomic temperature, stress and strain.

Babić et al. [13] discussed the drilling and dicing issues related to GaN-on-diamond wafers using laser micromachining for radio frequency power transistor applications.

Gu et al. [14] reported the use of pulsed UV lasers for the manufacturing of microstructures for GaN in free standing state and were succeeded to create good quality trenches for free-standing GaN.

Nowak et al. [15] applied contact loading of the surface called as c and m and captured the response of homoepitaxially created GaN when it deformed on a nano scale.

Guo et al. [16] studied Ga and N faced GaN in terms of their nanotribological properties using diamond indenter through nano-scratch experiments and suggested that the modulus of elasticity of Ga faced GaN was little bit higher than the N faced GaN.

Zou et al. [17] executed research on the impact of mechanical action and chemical function, during the chemical-mechanical polishing (CMP) process on the pits that appear on the GaN surface after polishing. The association between surface characterization after CMP of GaN substrates and the concentration of the silica ($SiO2$) abrasive employed for CMP was studied.

Qian [18] observed the deformation in wurtzite GaN through molecular dynamics simulations. Slips on the planes were calculated by the investigation of generalized stacking fault energy.

Xiang et al. [19] formulated research with the help of molecular dynamics on B4 ceramic to examine the creation of prismatic loops on it due to nanoindentation.

Wang et al. [20] described that the failure mechanisms are dependent on size and the shuffle set pyramidal planes after carrying a study on the examination of the GaN nanowires about their mechanical responses, especially in their inelastic range.

Aida et al. [21] revealed the scientific relation between the diamond abrasive size which was used for GaN substrates for mechanical polishing and depth of the subsurface damage (SSD) and listed that SSD depth decreases as the diamond abrasive reduces in size.

2.4 Motivation

Considerable literature has been published using molecular dynamics approach for the machining of GaN numerically, therefore in the present research, we establish a new 3d smoothed particle hydrodynamics model of diamond cutting of GaN based on the Mohr-Coulomb material model which can capture plastic flow and brittle failure. We also find out the cutting forces present during machining process by these numerical simulations.

CHAPTER 3: MANUFACTURING

3.1 Manufacturing and its types

Manufacturing is the process of making desired goods or finished goods from raw materials or parts using machinery tools, human labor and chemical processing. It can be divided into following categories.

- Jobshop manufacturing

- Repetitive manufacturing

- Discrete manufacturing

- Batch manufacturing

- Continuous process manufacturing

- 3d Printing

Figure 7: Car Manufacturing Plant [22]

3.1.1 Jobshop manufacturing

In jobshop manufacturing, instead of an assembly line, production areas are used for small batch, count of which depends upon the order received by the company. This type of manufacturing is suitable for one product or a handful of them like a custom jacket maker or custom sports accessories maker. Many of such firms can be used to manufacture industrial parts for different firms or industries.

3.1.2 Repetitive manufacturing

In repetitive manufacturing, as the name suggests, this technique is useful to produce repeat products at a defined production rate. This production method has production lines making the same good repeatedly depending upon the requirements or demand of the client or industry. Companies like this include automobiles, electronics and specific consumer goods.

3.1.3 Discrete manufacturing

Discrete manufacturing is different from repetitive manufacturing in a way that it allows the frequent change over and variations in the good/product being manufactured. Such a company can afford multiple sizes designs or modifications offer the same product, but it may require more time according to the set up or removal as required.

3.1.4 Batch manufacturing

Batch manufacturing has similarities with both discrete and job shop manufacturing processes. Such a manufacturing technique is driven by the order received by the firm or company, after one desired batch is produced the setup is cleaned and it can be resumed once the buyer needs another batch.

3.1.5 Continuous Process manufacturing

Continuous process manufacturing shares many functions like repetitive manufacturing. However, the difference is that the raw materials used are often slurry, liquids or powders. Such companies include food products like sauces and ketchups.

3.1.6 3d Printing

3D printing is considered as a manufacturing process and has very wide use. It was developed around 1980s and now it has capabilities to make even 3-dimensional houses, layer by layer using a digital model. Various composites and metals are used as raw materials.

Figure 8: 3d printing of a bolt being done [23]

3.2 Production Engineering

Production engineering consists of metal cutting tools, boring, grinding, and analysis of cutting forces.

Figure 9: Material undergoing a machining process on CNC Lathe [24]

There are two types of metal cutting called orthogonal and oblique cutting. Orthogonal cutting is often called 2-dimensional cutting and oblique cutting also known as 3-dimensional cutting. In orthogonal cutting, the edge of the cutting tool makes right angle with the tool velocity vector. In oblique cutting, the tool's cutting edge forms an angle less than right angle to the velocity vector of tool as shown in picture given below.
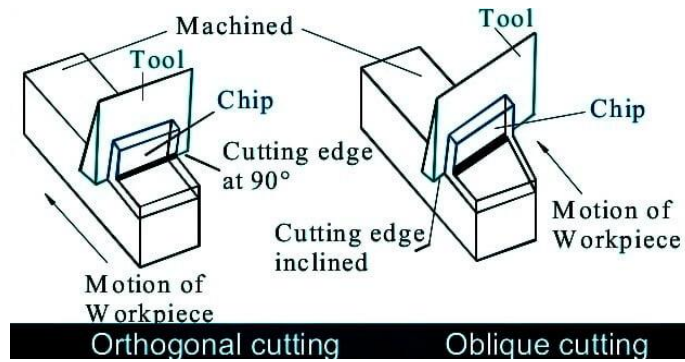
Figure 10: Orthogonal vs Oblique cutting [25]

3.2.1 Types of chips during machining

There are three types of chips produced during the machining process.

- Discontinuous chips

- Continuous chips

- Continuous chips with built up edge

3.2.1.1 Discontinuous chips

These chips are formed as a result of the machining of brittle materials like costiera. Their discontinuous chips are made due to low cutting speed and small rake angle of the tool.
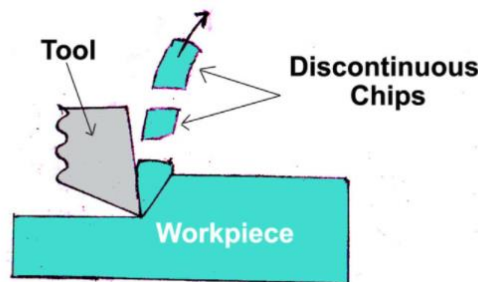
Figure 11: Formation of Discontinuous chips during machining [26]

15

3.2.1.2 Continuous chips

These are produced when ductile materials are machined like mild steel. The continuous chips are made due to large rake angle and high cutting speed of the tool. These chips have approximately same thickness and have long coils.
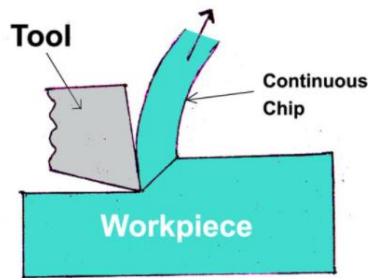
Figure 12: Formation of continuous chips during machining [26]

3.2.1.3 Continuous chips with built up edge

Such chips are formed when the rake angle of the tool is small and cutting speed is low during the machining of ductile materials. Dull cutting edge of cutting tool is also responsible for the formation of such chips.
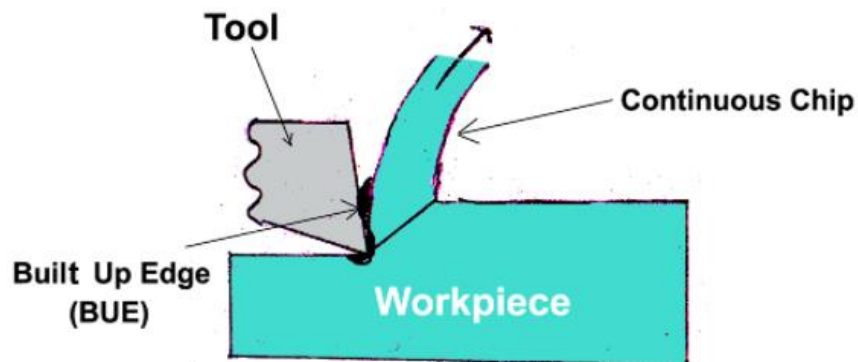
Figure 13: Formation of continuous chips with buildup edge during machining [26]

3.2.2 Single Point Cutting Tool

Lathe, shapers and planer machines usually use a single point cutting tool whereas broaching machine and milling machine use multi point cutting tool. Single point cutting tool maybe a left hand or right hand depending upon feed direction.
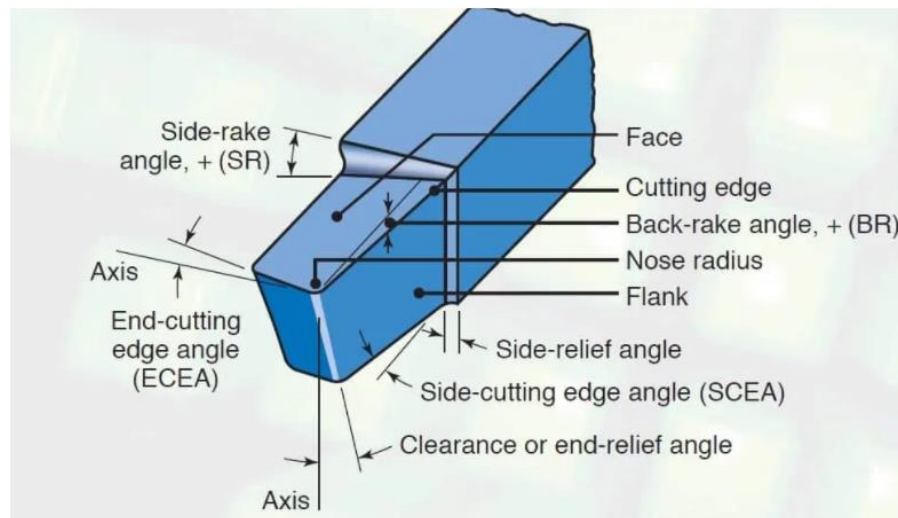
Figure 14: Nomenclature of Single Point Cutting Tool [27]

Nomenclature of the single point cutting tool is listed below.

Shank: main body of tool

Face: chip sliding surface

Flank: surface below and adjacent to the cutting edge

Heel: intersection of the base of tool and the flank

Nose: intersection of end cutting edge and side cutting edge

Cutting edge: edge of the face which removes the material from the workpiece

Side cutting edge angle: the angle between side of the tool shank and side cutting edge

End cutting edge angle: angle made by line normal to tool shank and the end cutting edge.

End relief angle: angle made by line perpendicular to the base of the tool and the portion of the end flank immediately below the end cutting edge

Back rake angle: the angle made by the plane parallel to the base of the cutting tool and the face of the tool. The strength of the tool depends on the rake angle.

Side rake angle: angle made by the line parallel to the base of tool with the tool face i.e., it represents the slope of the face of the tool from the cutting edge.

3.3 Modern machining processes

In modern machining processes, four fundamental types of machining energies like electrical, electrochemical, mechanical and thermoelectric are used for the workpiece and almost no physical contact is needed for the removal of material. Below are some types of modern machining processes. Some types of modern machining processes are

- Ultrasonic machining
- Electrochemical machining
- Electro-discharge machining

3.3.1 Ultrasonic machining

Any abrasive slurry between the tool and workpiece can be used to remove the metal in ultrasonic machining. By abrasion, thousands of microscopic aggressive grains are removed by the vibratory tool made of brass or copper. Usually, this type of machining is best applicable for glass plastics tool steels etc. Brittle materials can also be machined by this machining process. Good surface finish is produced as it cuts materials at very low speeds.

Figure 15: Ultrasonic Machining being done[28]

3.3.2 Electrochemical machining

An electrolyte is maintained between the tool and workpiece in a very small gap about 0.75 millimeter and hence the metal is removed. The electrolyte mostly used is the solution of sodium chloride in water.

Figure 16: Electrochemical machining being done [29]

3.3.3 Electro-discharge machining

In Electro discharge machining, a rapidly recurring spark discharges between the tool which is used as cathode and workpiece which is used as a node separated by flooded dielectric flute through a small gap end results in metal removal. This type of machining produces high degree of surface finish and can machine many hardest materials.
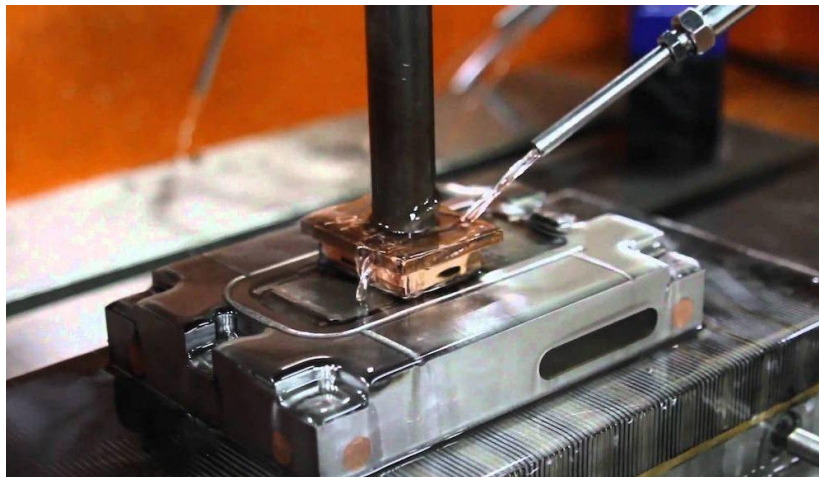
Figure 17: Electro-discharge machining being done [30]

CHAPTER 4: NUMERICAL METHODS

Exact solutions in many engineering problems are often difficult to find. Generally, this difficulty is aroused due to the complexity of governing differential equations or the complex boundary and initial conditions. Numerical methods help us to solve such problems. Analytical solutions provide exact solution whereas numerical methods approximate the exact solutions only at discrete points called nodes. The first step in any numerical procedure is to divide the medium of interest into small subregions called elements and nodes. Two main categories of numerical methods are finite difference methods and finite element methods. In finite difference methods both equations are written, and the derivative parts are replaced by difference equations. This method is suitable for simple problems, but they are not suitable for complex geometries and boundary conditions. Integral formulations rather than different situations are used by finite element method to provide the approximate solution for each element which is integrated later for the whole assembly.

4.1 Finite Element Method (F.E.M) and ANSYS/LS-DYNA

Many problems in engineering can be solved by applying the finite element method which is a numerical procedure. Finite element methods can analyze linear, nonlinear, transient problems in fluid flow, heat transfer, stress analysis and electromagnetism. The modern finite element method was found in the early 1900s when some researchers approximated elastic continuum using discrete equivalent elastic bars. However, first person to develop the finite element method was Currant 1943, piecewise polynomial interpolation was used by Currant in early 1940s who

investigated story and problems in a paper he published. ANSYS was released in 1971 for the first time. It is very robust and vast general purpose finite element computer program which consists of more than one Lac lines of code. Any type of analysis from static to dynamic, heat transfer to fluid flow, and electromagnetism can be solved using ANSYS/LS-DYNA. From about 30 years, ANSYS has been the leader in finite element analysis domain. However, it is beneficial to have basic knowledge of finite element analysis before using any FEM commercial package.

4.2 Basic steps in F.E.M

- Preprocessing phase

- Solution Phase

- Postprocessing phase

4.2.1 Preprocessing phase

1. The problem domain is divided into small subregions called elements and nodes.

2. The physical behavior off an element is represented by an assumed shape function that approximate behavior of an element.

3. Equations for an element are developed.

4. Then elements are assembled, and global stiffness matrix is formed.

5. Apply loading, initial conditions and boundary conditions.

4.2.2 Solution phase

In solution phase, the algebraic equations are simultaneously solved to obtain the nodal results. These equations maybe linear or nonlinear depending upon their physical behavior.

4.2.3 Post processing phase

The output values, for which the solution was solved, in which doer is interested in getting them are viewed with the help of colorful images, charts, graphs etc.

4.3 F.E.M Formulations

Usually, there are three types of formulations used to formulate the finite element analysis problems, but the steps listed above remains the same regardless of which type of formulation is used.

- Direct formulation
- Variational approach
- Weighted residual approach

4.3.1 Direct formulation

The direct formulation is linked with direct stiffness method of the structural analysis, and it is the simplest to understand while using FEM at beginner stage. It teaches the amateur analyst the basic techniques and essential concepts involved in FEM without getting deeper into mathematics. Besides its simplicity, the downside is it is only limited for very simple problems. It starts with the replacement of under consideration system with the equivalent idealized system of

individual elements, attached with one another on points called nodes. Desired set of equations are defined at single element then they are assembled for the whole assembly and solved for the unknown nodal entities.

4.3.2 Variational Approach

In this approach the problem is defined using some variational principle like principle of minimum potential energy. Whenever a classical variational statement is present for the physical problem, finite element equations are derived using this approach. Variational approach uses a basic range of calculus of variations. The disadvantage to this approach is that many problems lack the variational statement and hence this method can't be applied on such problems. For example, in the case of most of the nonlinear problems, variational approach is not helpful. Variational formulation uses the Rayleigh-Ritz method as an approximate method.

4.3.3 Weighted residual approach

Usually, most of the differential equations are solved approximately by WRM. This method is applicable for both linear and nonlinear analysis. It consists of two main steps, in the first step approximate solution is assumed for the behavior of the system. Such solution satisfies the boundary conditions for the desired variable. In second step, those created equations from the first step are solved.

4.4 Smoothed Particle Hydrodynamics (S.P.H)

Physical problems like fluid flow and transport phenomena are mostly modelled in the Eulerian framework. This modelling approach, utilized in numerical techniques such as the finite difference method, finite volume method and finite element method, requires the use of grids or meshes to

solve integral formulations or partial differential equations. Controlling consistency is one of the problems while using approaches that use meshes. This difficulty can especially arise when dealing with complex geometries, mobile interfaces, free surfaces, and topological changes. Remeshing can be done to address these problems, but it is expensive and time-consuming.

In lagrangian modelling, the system can be subdivided into particles that are finite and in their original intent, they do not share any information with each other. Coordinates of centre of mass define the position and their physical properties as well. These meshless approaches are being widely used for research purposes resulting in accurate and stable solutions for partial differential equations or integral formed equations. In the previous decade or so, there is a sudden increase in the use of meshless methods for complex problems. Smooth particle hydrodynamics (SPH), Least squares (MLS), and Galerkin method are some of the extensively used meshless numerical methods [31].

In the late 1970s, astrophysics phenomena were studied by Lucy et al. [32] and Ringold et al. [33] by using SPH method for the first time. Later, due to its ability to accommodate the complex attributes of physical problems, it was applied to solid and fluid mechanics problems as well [31] . The basic underlying rule is to subdivide the system into particles. Weighted interpolations are used to give properties to these particles which are in the neighbourhood defined by the domain of influence. The response of the physical quantities in the fixed particle is dependent on the neighbouring particles which are at a radial distance from it as shown below in Fig.31.
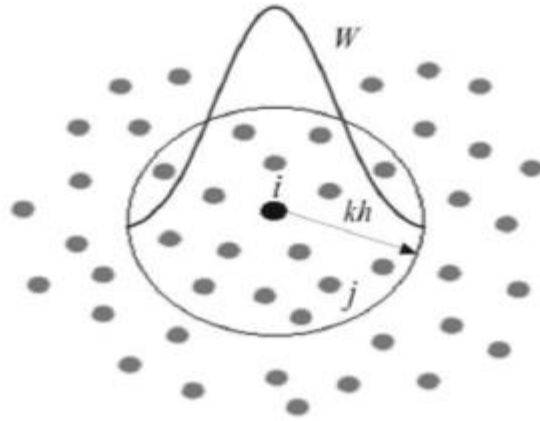
Figure 18: Graphical representation of the kernel and its dominance domain. Physical properties of the reference particle 'i' is affected by the side particle 'j' which lies inside the influenced area [31]

General mathematical expression for SPH method is given below

$$f_i = \sum_{j=1}^{n} m_j \frac{f_j}{\rho_j} W(X_i - X_j, h) \tag{1}$$

Where in (1)

f_i Fixed particle's approximated value

f_j Neighboring particle's approximated value

m_j Neighboring particle's mass

ρ_j Neighboring particle's density

X_i Fixed particle's location

X_j Neighboring particle's location

$W(X_i - X_j, h)$ Value of kernel found at the respective location

26

n   total number of particles acting as neighbors

4.5 Mohr-Coulomb Material Model

The Mohr-Coulomb material model is extensively used in geomechanics. Rock, soil, and aggregate materials are modeled by this method to show their mechanical behavior in their natural or artificial ambience. Masonry structures made of concrete and similar materials, which fail due to stress concentrations or because of weak regions, can be effectively modeled by this material model. Examples of such structures include footings, pilings, and seismic systems.

Plastic deformation after an initial elastic stage is displayed by materials that follow the Mohr-Coulomb material model. Unloading from the plastic deformation results in the recovery of elastic stage. Phenomena such as shear loading and volumetric plasticity, realized when the particles move past one another in a domain can be traced back to the material behavior at the microscopic level. Plastic deformations start when the internal friction among particles is dominated by the shear force applied. Being a wurtzite crystal, GaN suits the applicability of this method. Normal force between the particles defines the frictional resistance of such materials which can be modeled by Mohr-Coulomb material model [34]. Material data for GaN were taken from GRANTA/ANSYS Library [35].

Mathematically, Mohr-Coulomb material model is represented by the following equations

$$| \tau | = S_\circ + \sigma \tan\phi \qquad (2)$$

$$(\sigma_1 - \sigma_3) = (\sigma_1 + \sigma_3) \sin\phi + 2S_\circ\cos\phi \qquad (3)$$

$$\tau_m = f(\sigma_m) \qquad (4)$$

Where

τ Shear stress

$S_{\circ}$ Inherent shear strength of material also called cohesion value

σ Normal stress

ϕ Internal friction angle

σ_1 Major principal stress

σ_3 Minor principal stress

τ_m Mean shear stress

σ_m Mean principal stress

α_f Angle between minor principal stress plane and failure plane

When represented in Mohr diagram, Eq. 2 is a straight line at a friction angle ϕ from the normal stress plane σ as shown in Fig. 3. Eq. 3 is an alternative form of Eq. 2 which can be obtained by making the Mohr circle tangent to the line which has a stress state linked with failure. Eq. 4 shows that on the $\tau - \sigma$ plane, the Mohr envelope can be constructed and the tangency of the circle having diameter $(\sigma_1 - \sigma_3)$ to the failure envelope $\tau = g(\sigma)$ will result in failure.
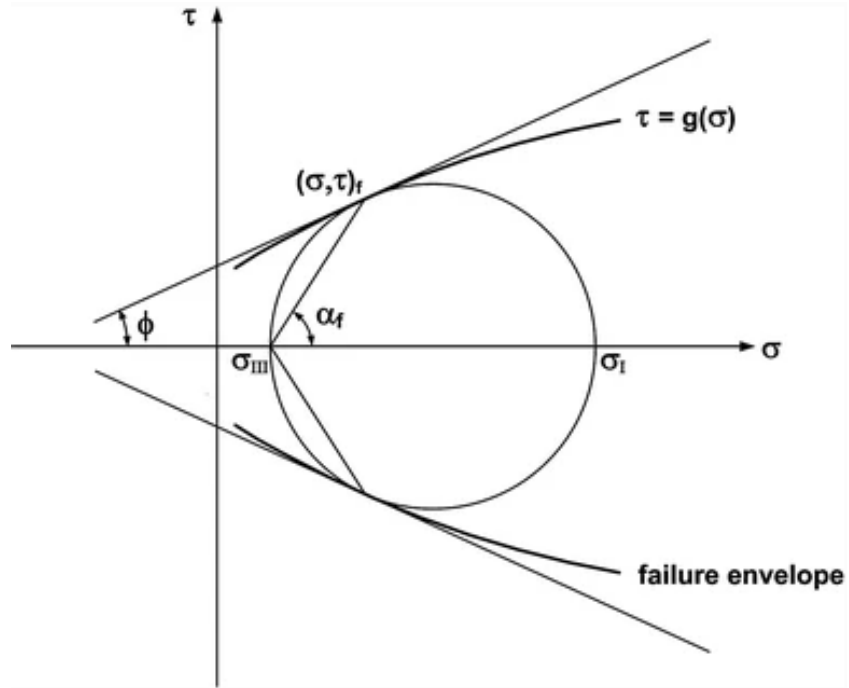
Figure 19: Mohr Diagram and failure envelops [36]

4.6 Johnson Cook Material Model

The Johnson Cook Material Model is composed of two subsets called Johnson Cook Strength and Johnson Cook Failure explained below.

4.6.1 Johnson Cook Strength

Strength behavior of materials specially metals are represented by this material model when they undergo excessive strains, strain rates and temperatures. Some problems of intense impulsive loading may be seen due to some high velocity impacts during the simulation.

Yield stress is defined by the model as

$$Y = [A + B\varepsilon_p^n][1 + C\backslash ln\varepsilon_p^*][1 - T_H^m] \qquad (5)$$

Where

ε_p is effective plastic strain

ε_p^* is normalized effective plastic strain rate

T_H is homogeneous temperature i.e. $\frac{T - T_{room}}{T_{melt} - T_{room}}$

A,B,C,n and **m** are material constants

Stress as a function of strain is given by the first set of brackets when (for laboratory experiments) $\varepsilon_p^* = 1$ sec^{-1} and $T_H = 0$. Effect of strain hardening is represented by B and n whereas basic yield stress at low strains is represented by A.

Effects of strain rate on the yield strength is shown by the second set of brackets. Plastic strain rate enhancement is normalized using the reference strain rate against which the material data was measured.

Thermal softening is represented by the third bracket set such that, at the melting temperature T_{melt} yield stress drops to zero.

4.6.2 Johnson-Cook Failure

Ductile failure of materials experiencing high temperatures, pressures and strain rates can be effectively modeled by Johnson-Cook failure criteria. This model works like the Johnson-Cook plasticity model as it consists of the three independent terms. Pressure, strain rate and temperature terms collectively define the dynamic fracture strain as shown below by the mathematical equation

$$\varepsilon^f = \left[D_1 + D_2 e^{D_3 \sigma^*}\right]\left[1 + D_4 \ln|\dot{\varepsilon}^*|\right]\left[1 + D_5 T^*\right] \qquad (6)$$

Where

$\left[D_1 + D_2 e^{D_3 \sigma^*}\right]$: Pressure dependence

$\left[1 + D_4 \ln|\dot{\varepsilon}^*|\right]$: Strain rate dependence

$\left[1 + D_5 T^*\right]$: Temperature dependence

ε^f : Equivalent strain at failure

D_1, D_2, D_3, D_4, D_5 : Damage parameters or damage coefficients

σ^* : Triaxiality factor

$\dot{\varepsilon}^*$: Strain rate ratio

T^* : Temperature ratio

CHAPTER 5: NUMERICAL SIMULATION OF MACHINING OF STEEL AISI 1045

5.1 Basic Setup

A numerical/mathematical set-up was created inside ANSYS/LS-DYNA for the orthogonal cutting of Steel AISI 1045. A workpiece of dimension 10 mm by 3 mm was created with the Johnson-Cook material and failure model whereas its material properties were taken from [37] . Tool was treated as a rigid body with rake and relief angle of 15 degrees and 10 degrees respectively. Nose radius of tool was kept as 0.1 mm with a depth of cut of 0.15 mm. Tool's motion was controlled by defining a load curve. Obtained results of Effective Stress (Von-Mises) were persistent with the results from the literature. After verifying the results for steel AISI 1045 we proceeded for the machining of GaN. Basic set up of mathematical domain is shown below in Fig. 20.
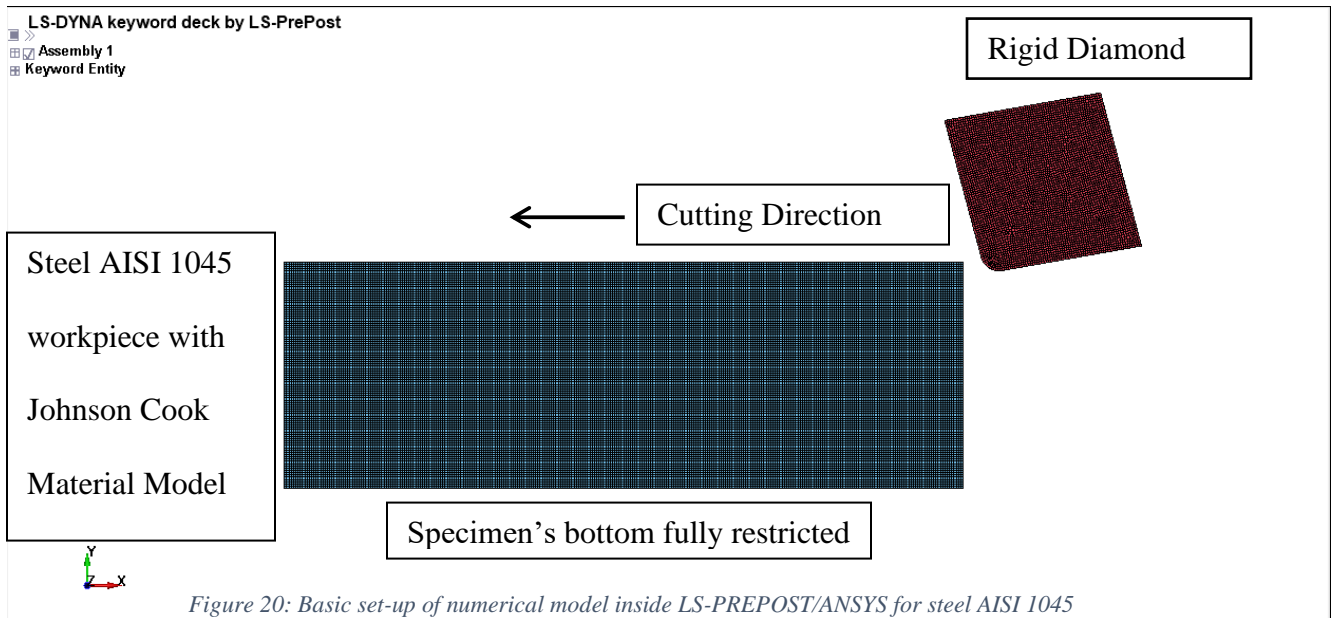
Figure 20: Basic set-up of numerical model inside LS-PREPOST/ANSYS for steel AISI 1045

5.2 Results and Discussion

Snapshots of stress distribution at different time intervals are shown by the figures from Fig. 21 to Fig. 24. It is obvious that effective Von-Mises stress increases as the tool progresses, shifting the very short-lived elastic deformation to plastic deformation. Once the Von-Mises stress reaches 1.090 GPa (1090 MPa), the material starts flowing plastically and chip formation starts. High stress zone can be seen in red in front of tool's cutting tip and some residual stresses can also be seen on the surface previously machined by the tool. Due to thermal softening and erosion of the elements, as the time progresses, the Von-Mises stress deviates negligibly from the initial stress value but remains closer to the flow stress value.

Figure 21: At t = 0 ms; Effective Von-Mises Stress = 0 GPa

Figure 22: t = 0.202 ms; Effective Von-Mises Stress = 0.4747 GPa
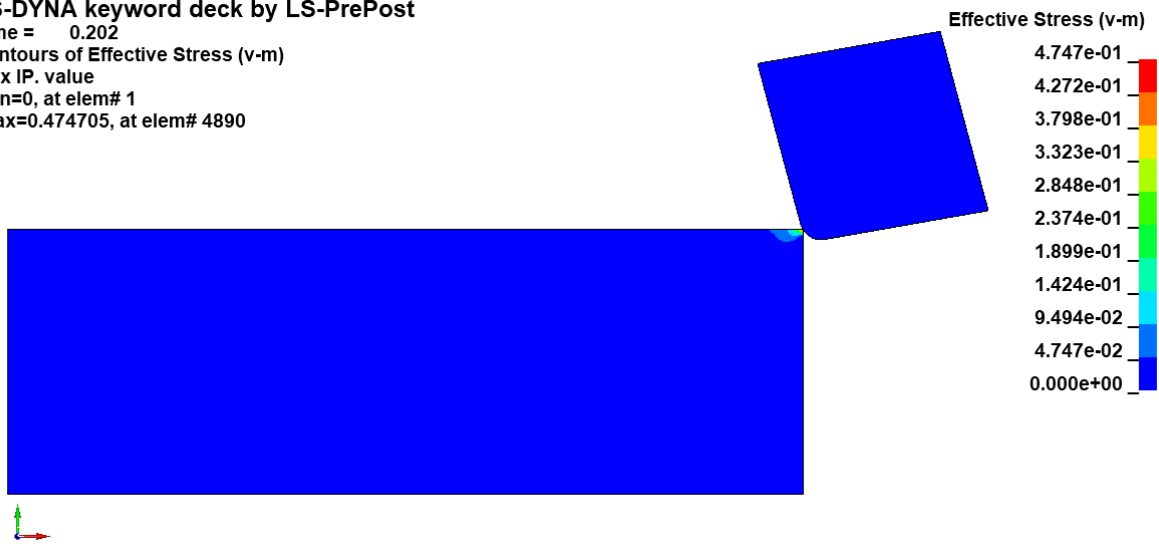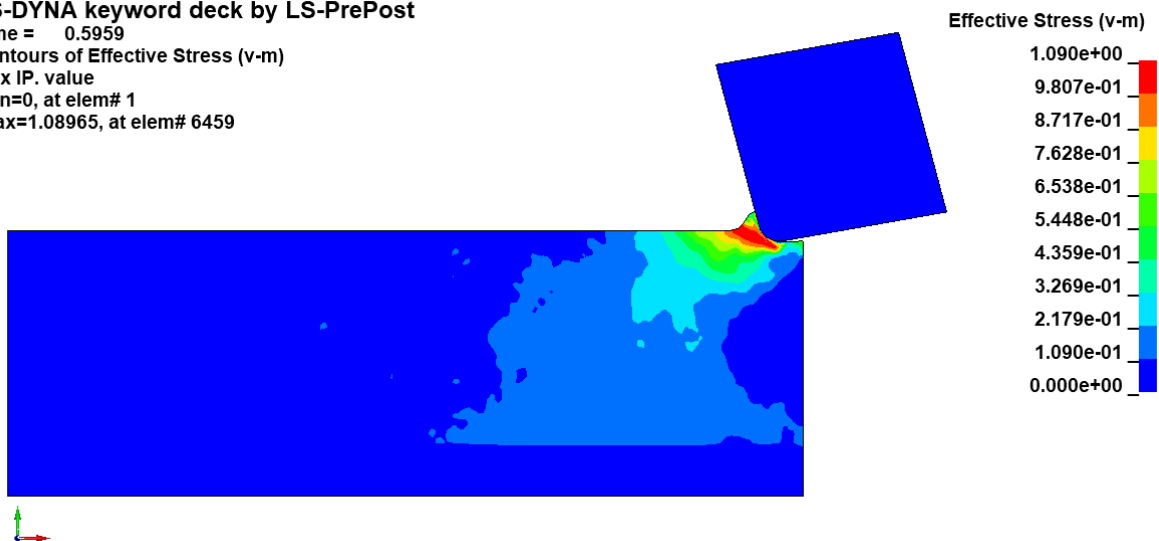

Figure 23: t = 0.5959 ms; Effective Von-Mises Stress = 1.090 GPa

LS-DYNA keyword deck by LS-PrePost
Time =   0.79992
Contours of Effective Stress (v-m)
max IP. value
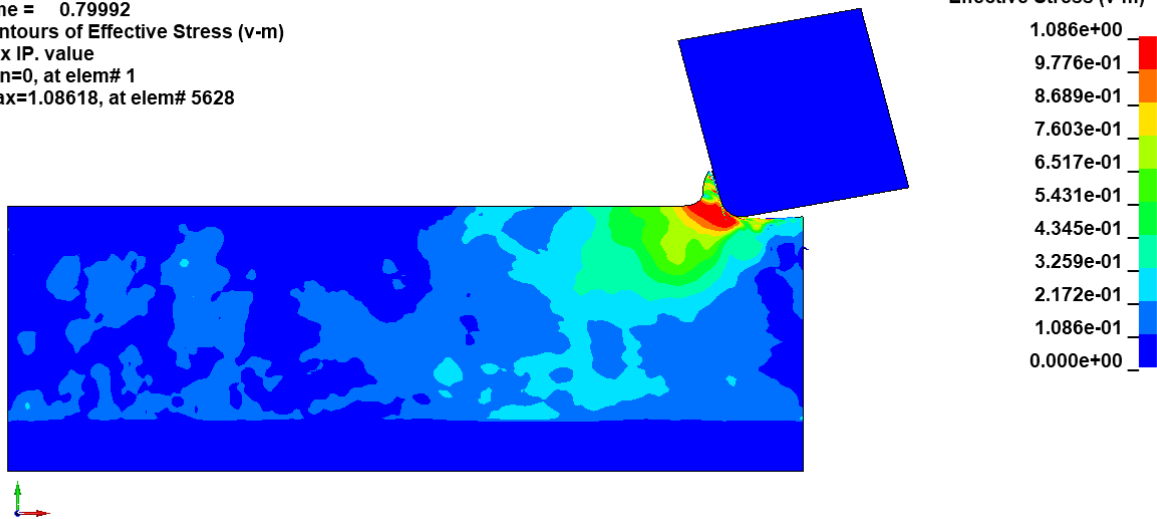 min=0, at elem# 1
 max=1.08618, at elem# 5628

Effective Stress (v-m)
1.086e+00 _
9.776e-01 _
8.689e-01 _
7.603e-01 _
6.517e-01 _
5.431e-01 _
4.345e-01 _
3.259e-01 _
2.172e-01 _
1.086e-01 _
0.000e+00 _

Figure 24: t = 0.79992 ms; Effective Von-Mises Stress = 1.086 GPa

Fig. 25 shown below, demonstrates an increasing trend in kinetic energy of the system as the tool progresses. After tool establishes the contact with the workpiece, kinetic energy starts to increase due to the forward movement of tool and a sharp increase in kinetic energy can be seen which may be due to the accumulation of the chip mass in front of the tool tip. Fig. 26 shows the change in the internal energy of the system which shows a rising tendency as well. Kinetic energy at every instance (point in time) remains less than ten percent of the internal energy which is also a useful check while validating the conducted analysis. Moreover, in Fig. 27 one can see that there is no abrupt change in step size (load step) during the simulation and it becomes stable at the end of the analysis.

From the simulation it is clear that effective Von-Mises stress once reaches 1090 MPa for steel AISI 1045, the ductile chip formation starts which matches with the flow stress value provided in Fig. 28 [38]i.e., 1120 MPa with an error of only 2.68%.
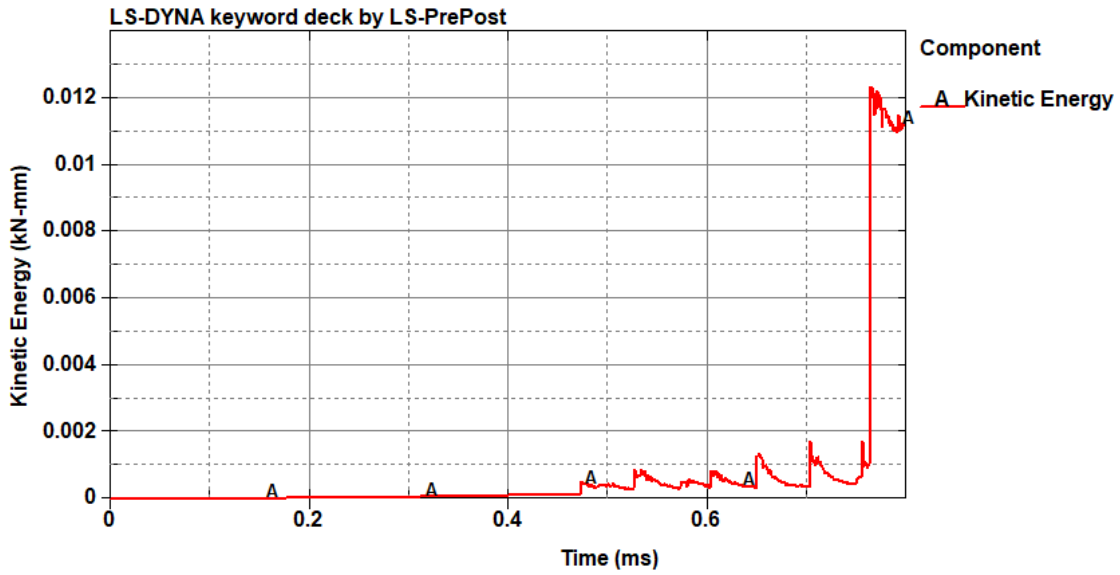
Figure 25: Graph showing change in Kinetic Energy with Time
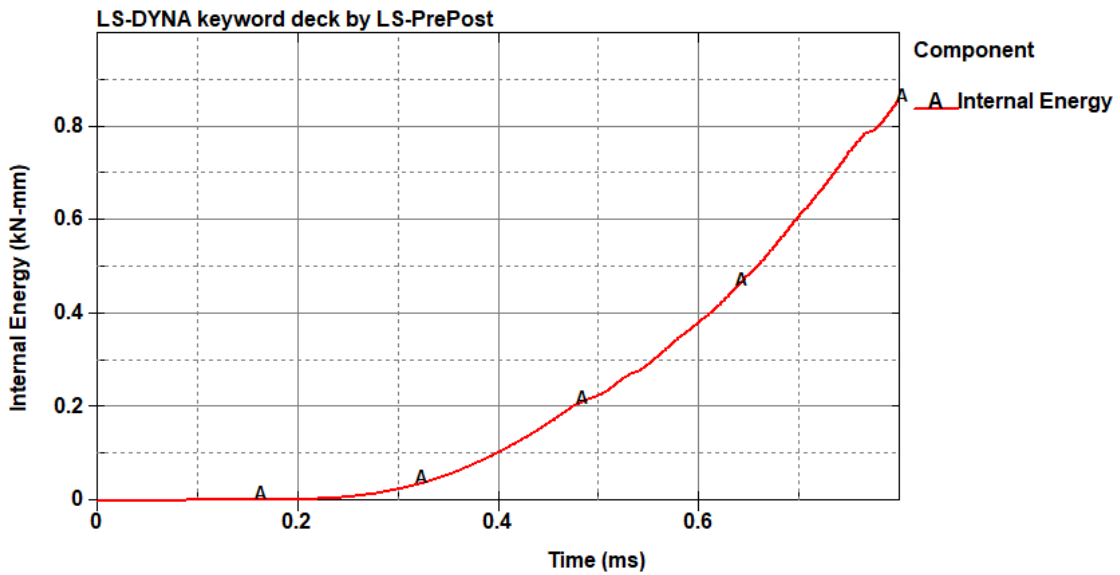

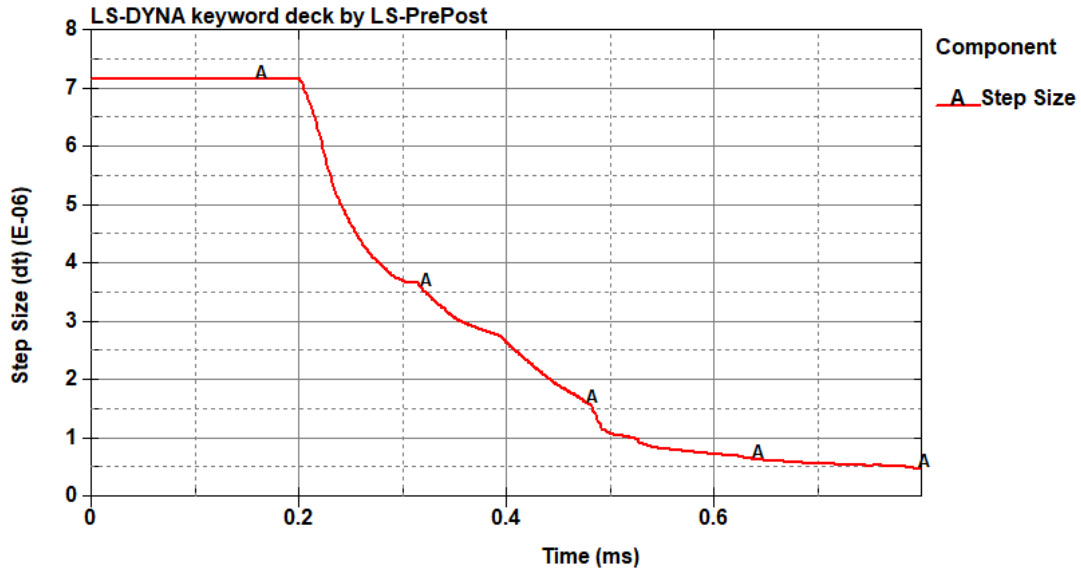*Figure 26: Graph showing change in Internal Energy with time*

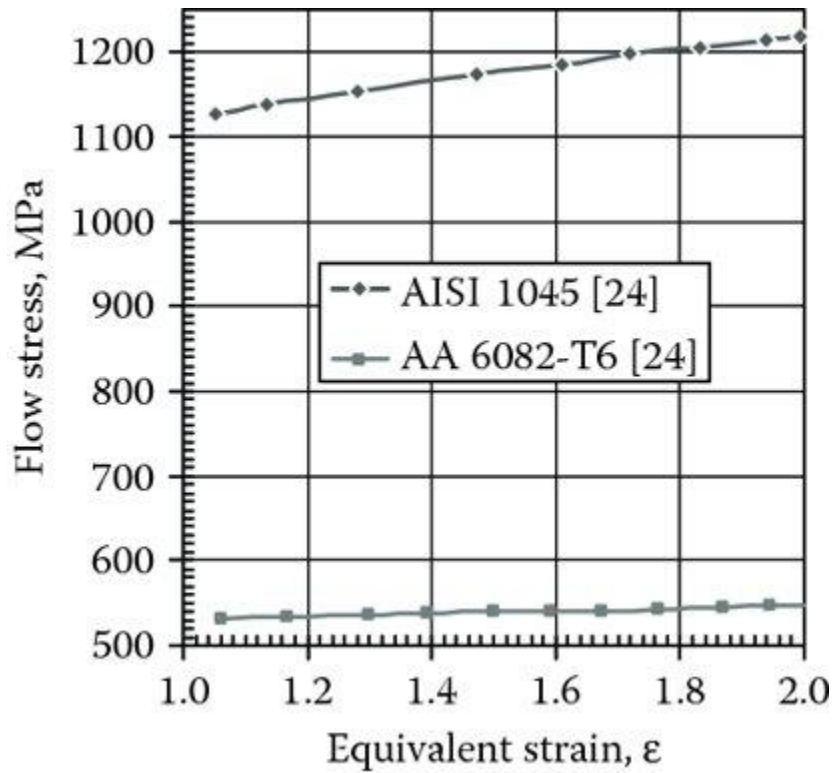*Figure 27: Graph showing variations in Step Size as time progresses*

Figure 28: Experimental graph showing Flow stress vs Equivalent strain for AISI 1045 and AA 6082-T6 [38]

CHAPTER 6: NUMERICAL SIMULATION OF MACHINING OF GALLIUM NITRIDE

6.1 Basic Setup

Fig. 29 shows a 3d model of orthogonal machining of GaN, which consists of a GaN workpiece and a diamond cutting tool inside ANSYS/LS-DYNA. The specimen has dimensions of 0.4 mm in length, 0.2 mm in height and 0.05 mm in thickness and SPH scheme is applied on it. The specimen's bottom is fully restricted in order to avoid any rigid body motion in the cutting process. The diamond cutting tool, being treated as rigid body, has a relief angle of 10°. Nose radius of tool is set as 0.01mm and rake angle is 15°.

Prior the cutting process, the tool tip is kept at an offset of 0.1 mm from the top right corner of the specimen with a 0.2 mm depth of cut. The tool movement is controlled by providing a load curve and it is expected that the specimen will deform from elastic stage to plastic stage and then brittle failure will occur.
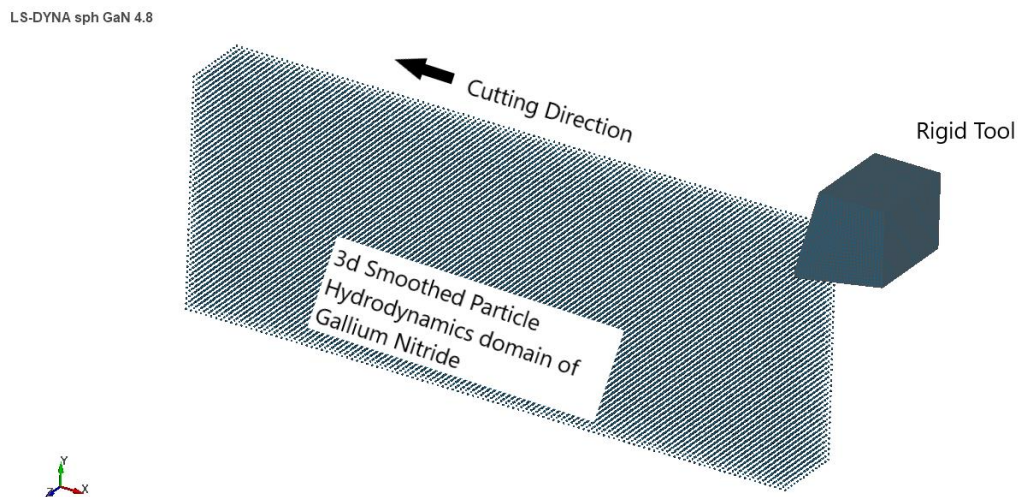

Figure 29: Basic set-up of Numerical Simulation in ANSYS/LS-DYNA

6.2 Results and Discussion

SPH simulation of orthogonal cutting was carried out to investigate the effective stresses, chip formation and cutting forces during conventional diamond tool cutting. Figs. 30 to 35 represent the snapshots of the process at different time intervals, showing the stress contours at various stages of the process. At the initial stages of the cutting process, there is no chip formation (Fig. 32), yet the material undergoes pure plastic deformation. High concentration of stress can be seen near the vicinity of tool tip. Upon further movement of tool along the cutting direction, there is a saw-tooth chip formed also called ductile mode cutting which immediately undergoes brittle material removal as shown in Fig. 33.

The local Von Mises stress distribution in the specimen changes with the progressive movement of the diamond tool. Stresses higher than 60 GPa are generated, which are concentrated ahead and underneath the cutting tip. Von Mises stress decreases after the passage of the tool in the machined area, leaving residual stresses behind.
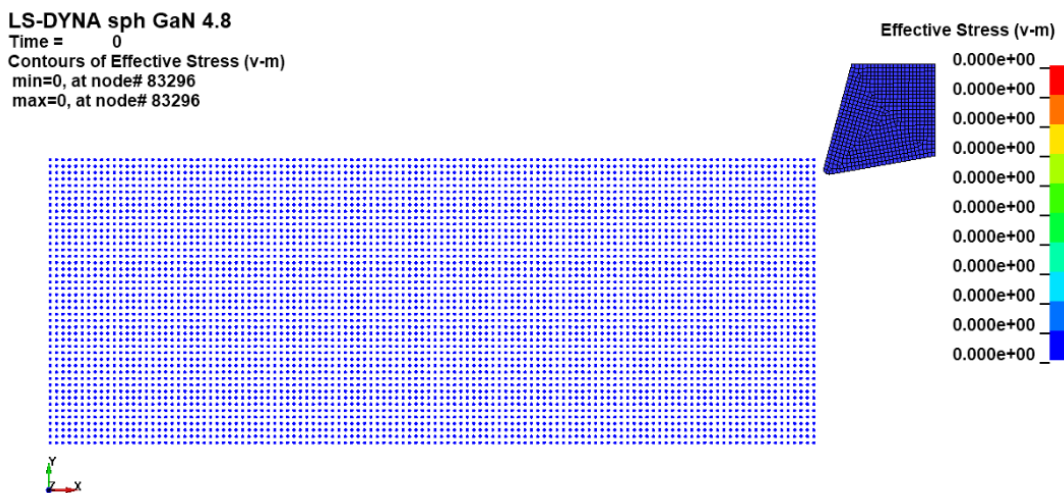
Figure 30: Maximum Stress = 0 GPa at time = 0 ms
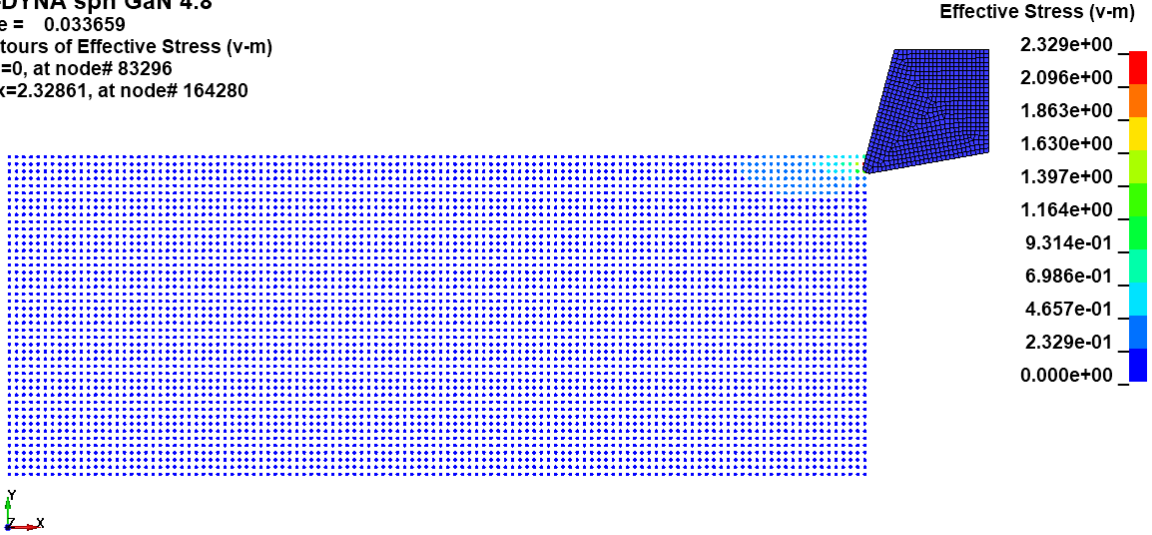
Figure 31: Maximum Stress = 2.329 GPa at time = 0.033659 ms
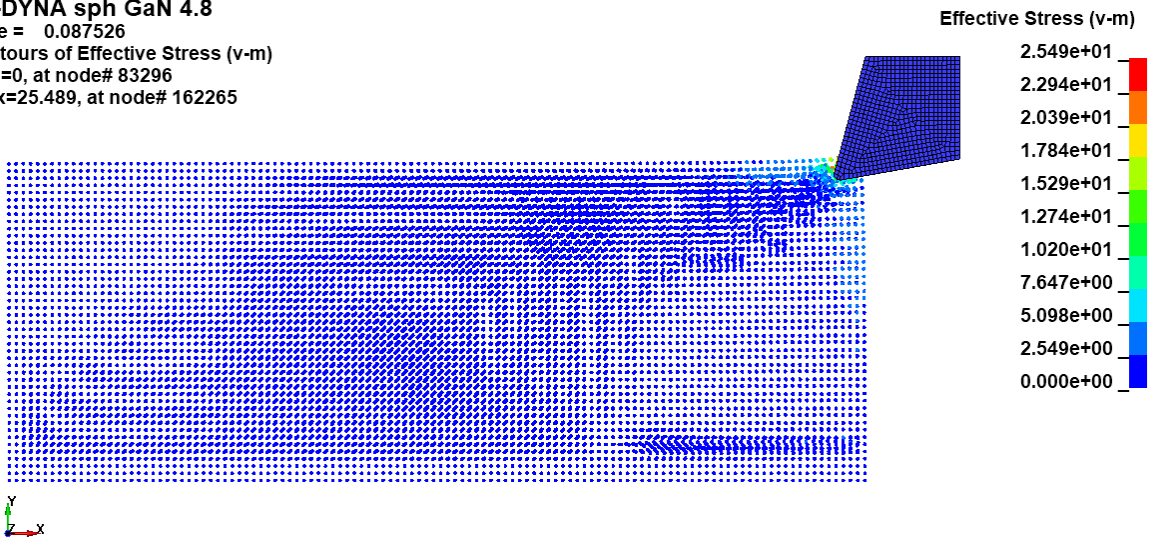
Figure 32: Maximum Stress = 25.49 GPa at time = 0.087526 ms
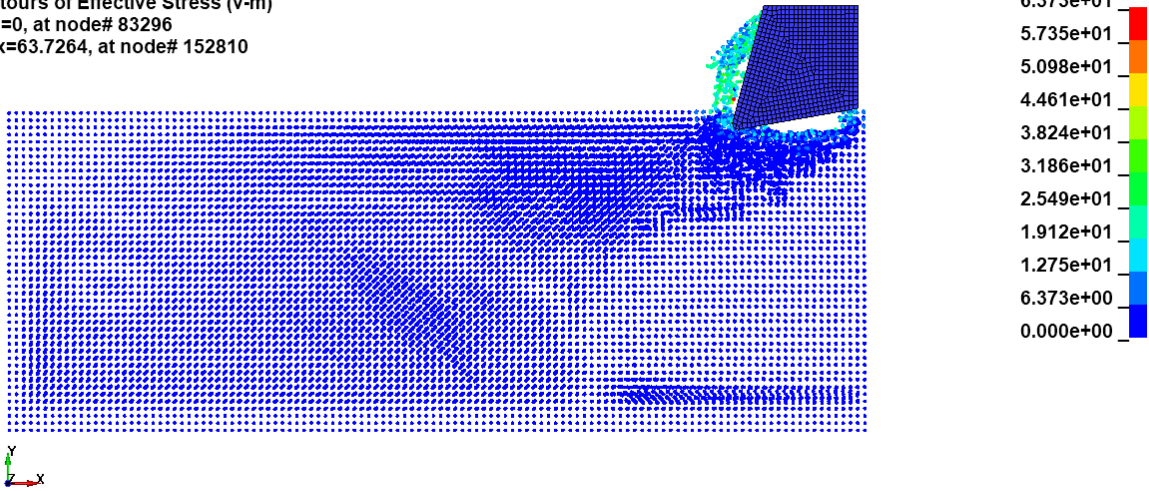
Figure 33: Maximum Stress = 63.73 GPa at time = 0.27606 m s
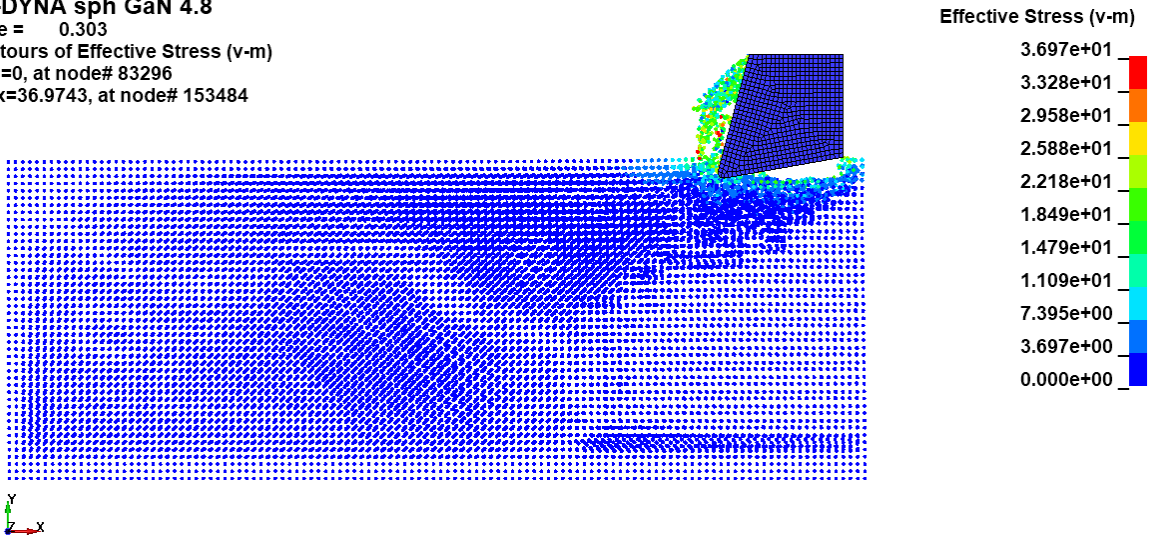
Figure 34: Maximum Stress = 36.97 GPa at time = 0.303 ms
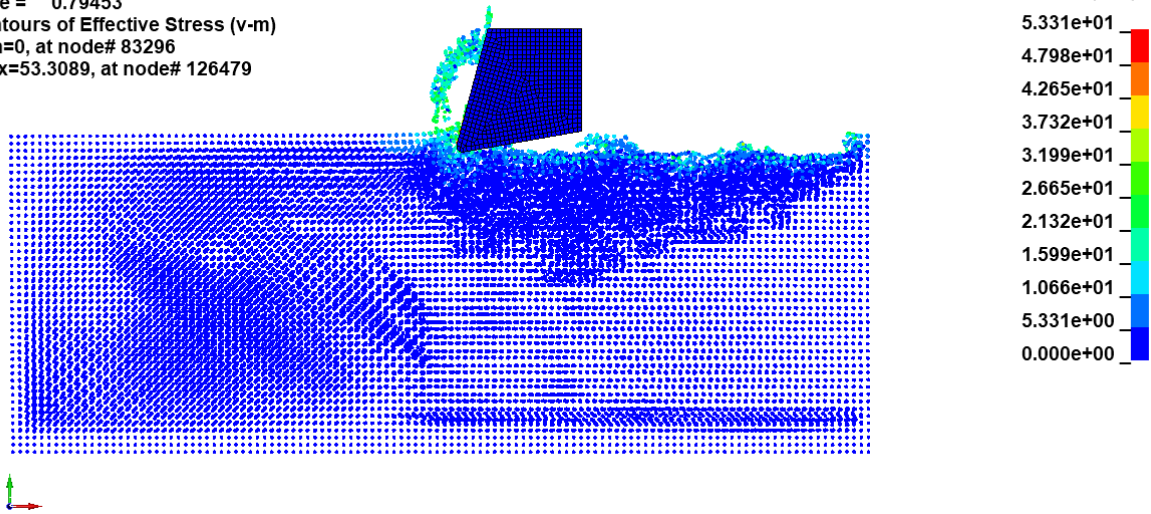
Figure 35: Maximum Stress = 53.31 GPa at time = 0.79453 ms

The contact force, as shown below in Fig. 36, with 0.02 mm depth of cut peaks at 2 kN but decreases to 1.83 kN when averaged over the total interval. However, this cutting force can be easily reduced by using small depth of cuts, slow movement of cutting tool along the cutting axis and decreased nose tip radius of tool.
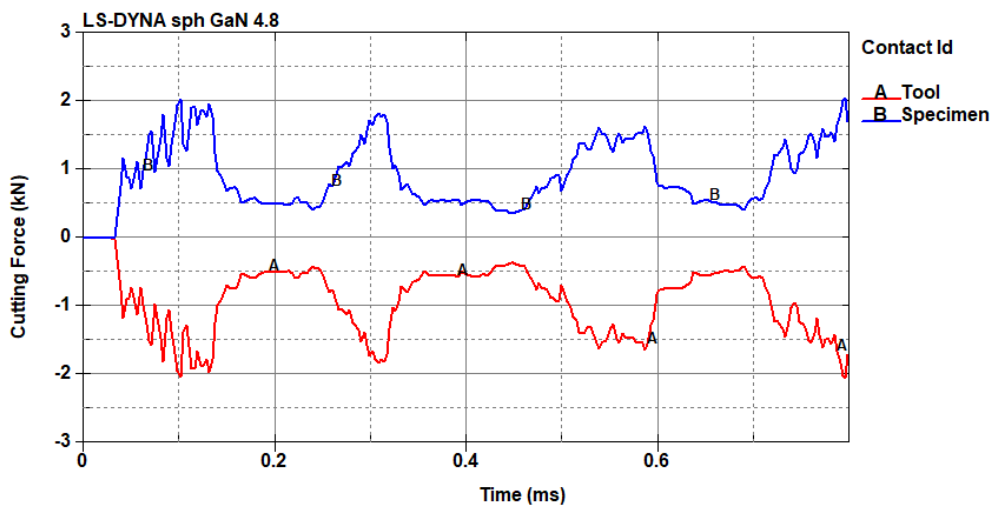
Figure 36: Graph showing cutting forces experienced by Tool and Specimen

Fig. 37 shows the behavior of kinetic energy during the simulation. Sudden establishment of contact between tool and workpiece creates first spike in kinetic energy which eventually decreases due to the dissipation of energy and erosion of elements. Once a bunch of SPH particles erode, kinetic energy rises again and repeat the erosion cycle. Fig. 38 shows the increasing trend of internal energy as solution progresses. Kinetic energy at every instance (point in time) is less than ten percent of the internal energy which is a useful criterion to judge for energy balance. Moreover in Fig. 39 step size has no abrupt values and stabilizes at the end as the time passes.
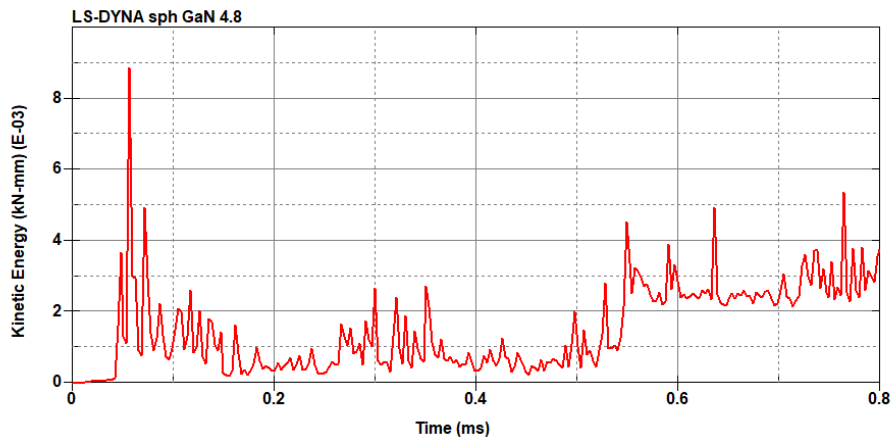
Figure 37: Graph showing changes in kinetic energy with time
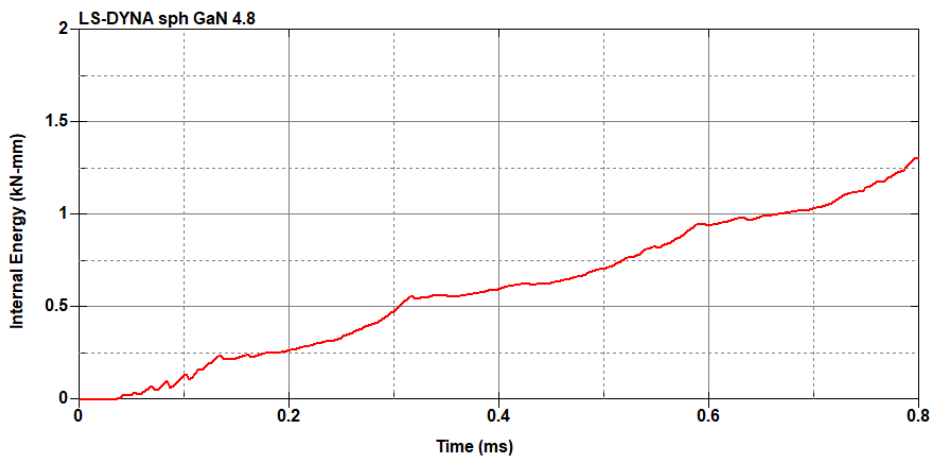
Figure 38: Graph showing changes in internal energy with time

43
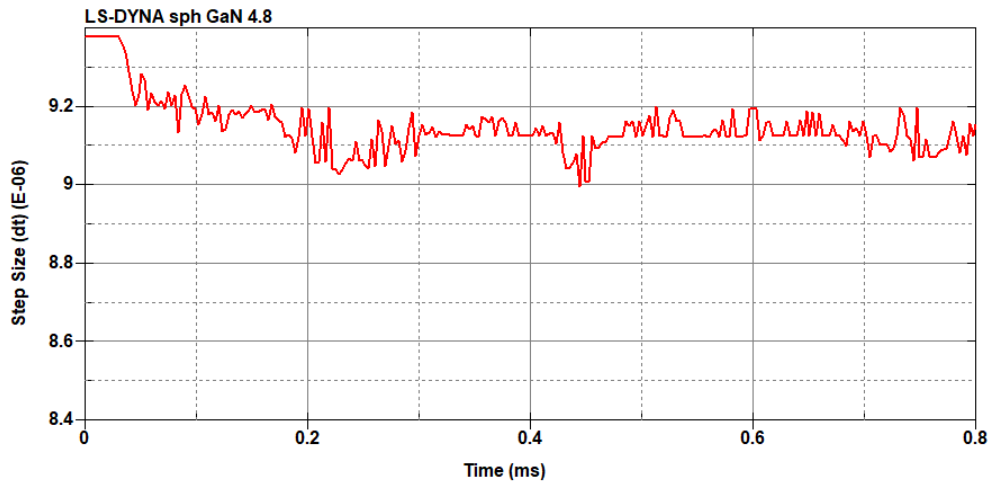
Figure 39: Graph showing change in step size with time

Fig. 40 shows the scattered graph showing the stress distribution inside the SPH domain of GaN as numerical simulation progresses. The small horizontal portion at the start of the simulation shows that the contact between diamond tool and the GaN workpiece has not been established yet. Once the tool comes in contact with the workpiece, the stresses pile up till point A. Once the Von Mises stress reaches point A, a sudden erosion of a bunch of SPH particles occur which can be classified as a dominant brittle failure which matches with the [39]. In the process, the stress decreases from 63.73 GPa to 38.2 GPa. For the next interval, due to the continuous forward movement of tool, equivalent stresses are again accumulated till point B and brittle failure occurs again resulting in lowering of the Von Mises stress. These cycles repeat till the end time of the simulation is reached. As the SPH approach is a particle-based approach, any particle reaching Mohr-Coulomb failure criteria will be eroded. An average peak value of equivalent Von Mises stress (at points A, B, C, and D) is found to be 58.2125 GPa at which brittle failure occurs which matches with the reported value of 64 GPa [39] with an error of 9.04% which is negligible.
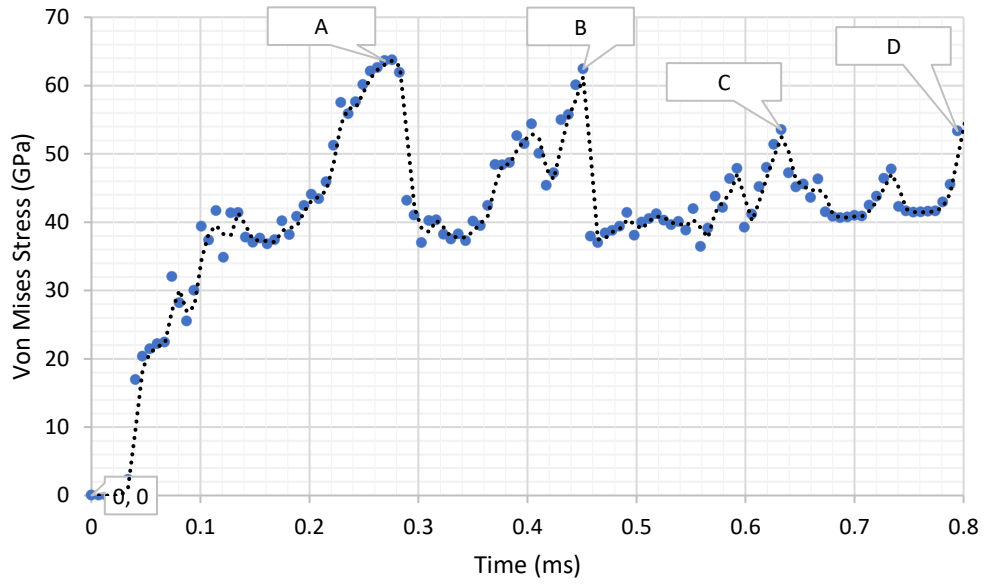
Figure 40: Graph showing Von-Mises stress vs Time
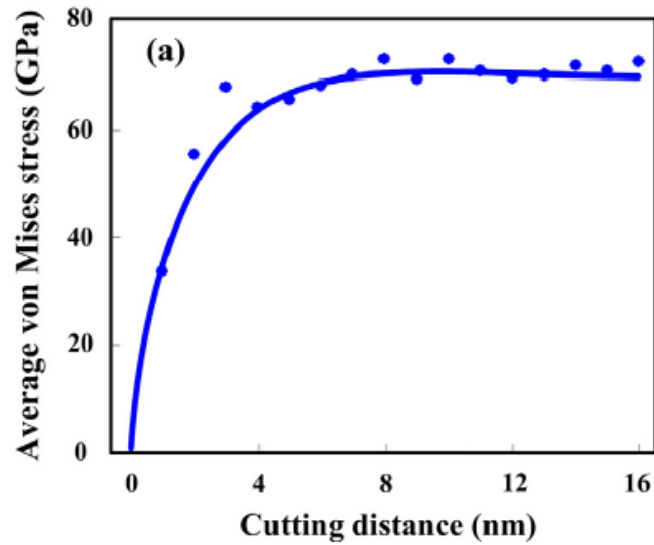
Figure 41: Graph showing average von Mises stress vs cutting distance [39]

45

CHAPTER 7

Conclusions and Future Work

7.1 Conclusions

This study demonstrates the feasibility of combining smoothed particle hydrodynamics with the Mohr-Coulomb material model to predict the machining behavior of Gallium Nitride as an alternate method to the computationally expensive Molecular Dynamics. As a further result of the framework developed, it is concluded that brittle mode material removal will be the primary cause of material removal during the orthogonal machining of Gallium Nitride.

7.2 Future Work

In future, suitable thermal criteria could be added to yield a more enhanced insight into GaN's material properties during different types of machining. This would also help in the optimization of the machining tool's parameters and surface finish of GaN.

REFERENCES

[1]   "Difference Between Ductile Material and Brittle Material."

        http://www.difference.minaprem.com/solid/difference-between-ductile-material-and-

        brittle-material/ (accessed Sep. 25, 2021).

[2]   "Electronica: Exagan demos multi-kW GaN PSUs."

        https://www.electronicsweekly.com/news/products/power-supplies/electronica-exagan-

        demos-multi-kw-gan-psus-2018-11/ (accessed Sep. 28, 2021).

[3]   "The Top 5G Use Cases — SDxCentral.com."

        https://www.sdxcentral.com/5g/definitions/top-5g-use-cases/ (accessed Sep. 28, 2021).

[4]   "How does radar work?" https://www.zmescience.com/science/how-does-radar-work/

        (accessed Sep. 28, 2021).

[5]   "Compact 3 kW on-board charger uses GaN transistors."

        https://www.smart2zero.com/news/compact-3-kw-board-charger-uses-gan-transistors

        (accessed Sep. 28, 2021).

[6]   "Infineon Gallium Nitride Power Devices - Electronics-Lab.com."

        https://www.electronics-lab.com/infineon-adds-gan-gallium-nitride-power-portfolio/

        (accessed Sep. 28, 2021).

[7]   E. Gu *et al.*, "Micromachining and dicing of sapphire, gallium nitride and micro LED

        devices with UV copper vapour laser," *Thin Solid Films*, vol. 453–454, pp. 462–466, Apr.

        2004, doi: 10.1016/J.TSF.2003.11.133.

[8]   T. Kim *et al.*, "Femtosecond laser machining of gallium nitride," *Materials Science and Engineering: B*, vol. 82, no. 1–3, pp. 262–264, May 2001, doi: 10.1016/S0921-5107(00)00790-X.

[9]   Y. Nakahama *et al.*, "Etching characteristics of GaN by plasma chemical vaporization machining," *Surface and Interface Analysis*, vol. 40, no. 12, pp. 1566–1570, Dec. 2008, doi: 10.1002/SIA.2955.

[10]   C. Zhang, Z. Dong, S. Yuan, X. Guo, R. Kang, and D. Guo, "Study on subsurface damage mechanism of gallium nitride in nano-grinding," *Materials Science in Semiconductor Processing*, vol. 128, p. 105760, Jun. 2021, doi: 10.1016/J.MSSP.2021.105760.

[11]   Y. Huang, M. Wang, Y. Xu, and F. Zhu, "Investigation of vibration-assisted nano-grinding of gallium nitride via molecular dynamics," *Materials Science in Semiconductor Processing*, vol. 121, p. 105372, Jan. 2021, doi: 10.1016/J.MSSP.2020.105372.

[12]   Y. Wang and J. Guo, "Effect of abrasive size on nano abrasive machining for wurtzite GaN single crystal via molecular dynamics study," *Materials Science in Semiconductor Processing*, vol. 121, Jan. 2021, doi: 10.1016/j.mssp.2020.105439.

[13]   D. I. Babić *et al.*, "Laser machining of GaN-on-diamond wafers," *Diamond and Related Materials*, vol. 20, no. 5–6, pp. 675–681, May 2011, doi: 10.1016/J.DIAMOND.2011.03.017.

[14]   E. Gu *et al.*, "Microfabrication in free-standing gallium nitride using UV laser micromachining," *Applied Surface Science*, vol. 252, no. 13, pp. 4897–4901, Apr. 2006, doi: 10.1016/J.APSUSC.2005.07.117.

[15] R. Nowak, "Nanoindentation study on insight of plasticity related to dislocation density and crystal orientation in GaN," *Applied Physics Letters*, vol. 101, no. 20, p. 201901, Nov. 2012, doi: 10.1063/1.4767372.

[16] J. Guo, C. Qiu, H. Zhu, and Y. Wang, "Nanotribological Properties of Ga- and N-Faced Bulk Gallium Nitride Surfaces Determined by Nanoscratch Experiments," *Materials 2019, Vol. 12, Page 2653*, vol. 12, no. 17, p. 2653, Aug. 2019, doi: 10.3390/MA12172653.

[17] Ariz. ICPT 2015 Chandler, American Vacuum Society Northern California Chapter, Center for Advanced Materials Processing, Institute of Electrical and Electronics Engineers, Ariz. International Conference on Planarization/CMP Technology 2015.09.30-10.02 Chandler, and Ariz. ICPT 2015.09.30-10.02 Chandler, "2015 International Conference on Planarization/CMP Technology (ICPT) Sept. 30, 2015-Oct. 2, 2015," 2015.

[18] Y. Qian, F. Shang, Q. Wan, and Y. Yan, "A molecular dynamics study on indentation response of single crystalline wurtzite GaN," *Journal of Applied Physics*, vol. 124, no. 11, p. 115102, Sep. 2018, doi: 10.1063/1.5041738.

[19] H. Xiang, H. Li, T. Fu, C. Huang, and X. Peng, "Formation of prismatic loops in AlN and GaN under nanoindentation," *Acta Materialia*, vol. 138, pp. 131–139, Oct. 2017, doi: 10.1016/J.ACTAMAT.2017.06.045.

[20] R. J. Wang, C. Y. Wang, Y. T. Feng, and C. Tang, "Mechanical responses of a-axis GaN nanowires under axial loads," *Nanotechnology*, vol. 29, no. 9, p. 095707, Jan. 2018, doi: 10.1088/1361-6528/AAA64D.

[21]   H. Aida *et al.*, "Evaluation of subsurface damage in GaN substrate induced by mechanical polishing with diamond abrasives," *Applied Surface Science*, vol. 292, pp. 531–536, Feb. 2014, doi: 10.1016/J.APSUSC.2013.12.005.

[22]   "Manufacturing | George W. Woodruff School of Mechanical Engineering." https://www.me.gatech.edu/manufacturing (accessed Sep. 28, 2021).

[23]   "3D printing and worker safety | 2019-04-28 | Safety+Health Magazine." https://www.safetyandhealthmagazine.com/articles/18295-d-printing-and-worker-safety (accessed Sep. 28, 2021).

[24]   "Machining and The Most Popular Machining Operations - Yena Engineering." https://yenaengineering.nl/machining-and-main-machining-operations/ (accessed Sep. 28, 2021).

[25]   "Difference Between Orthogonal and Oblique Cutting | Orthogonal Machining." https://mechanicaljungle.com/orthogonal-and-oblique-cutting/ (accessed Sep. 28, 2021).

[26]   "Types Of Chips in Metal Cutting - With detailed Diargram." http://www.mechanicalwalkins.com/types-of-chips-in-metal-cutting-and-factors-causing-them/ (accessed Dec. 06, 2021).

[27]   "Single Point Cutting Tool-Definition, Geometry, Nomenclature, Angle PDF." https://learnmechanical.com/single-point-cutting-tool/ (accessed Sep. 28, 2021).

[28]   "Ultrasonic-Assisted Machining with Standard Machines and Tools | Modern Machine Shop." https://www.mmsonline.com/articles/ultrasonic-assisted-machining-with-standard-machines-and-tools (accessed Sep. 28, 2021).

[29]   "Electrochemical Machining | Norwood Medical."
https://www.norwoodmedical.com/capabilities/electrochemical-machining (accessed Sep.
28, 2021).

[30]   "Electrical Discharge Machining: Principle and Manufacturing Applications."
https://www.rapiddirect.com/blog/what-is-electrical-discharge-machining/ (accessed Sep.
28, 2021).

[31]   C. Alberto. Dutra Fraga Filho, "Smoothed Particle Hydrodynamics : Fundamentals and
Basic Applications in Continuum Mechanics.," p. 167, 2018.

[32]   L. B. Lucy, Lucy, and L. B., "A numerical approach to the testing of the fission
hypothesis.," *AJ*, vol. 82, pp. 1013–1024, Dec. 1977, doi: 10.1086/112164.

[33]   R. A. Gingold and J. J. Monaghan, "Smoothed particle hydrodynamics: theory and
application to non-spherical stars," *Monthly Notices of the Royal Astronomical Society*,
vol. 181, no. 3, pp. 375–389, Dec. 1977, doi: 10.1093/MNRAS/181.3.375.

[34]   "Sample Libraries."
https://ansyshelp.ansys.com/account/secured?returnurl=/Views/Secured/corp/v202/en/wb_
eda/eda_ansys_matlib.html?q=geomechanical (accessed Aug. 28, 2021).

[35]   "Ansys Granta: Materials Information Management."
https://www.ansys.com/products/materials (accessed Aug. 29, 2021).

[36]   J. F. Labuz and A. Zang, "Mohr–Coulomb Failure Criterion," *Rock Mechanics and Rock
Engineering 2012 45:6*, vol. 45, no. 6, pp. 975–979, Jul. 2012, doi: 10.1007/S00603-012-
0281-7.

[37]   M. Murugesan and D. W. Jung, "Johnson cook material and failure model parameters estimation of AISI-1045 medium carbon steel for metal forming applications," *Materials*, vol. 12, no. 4, Feb. 2019, doi: 10.3390/ma12040609.

[38]   S. C. Veldhuis, M. M. Bruhis, L. S. Shuster, and G. S. Fox-Rabinovich, "Geometrical adaptation of cutting tools," *Self-Organization During Friction: Advanced Surface-Engineered Materials and Systems Design*, pp. 411–453, Jan. 2006, doi: 10.1201/9781420017861.CH13.

[39]   Y. Wang, S. Tang, and J. Guo, "Molecular dynamics study on deformation behaviour of monocrystalline GaN during nano abrasive machining," *Applied Surface Science*, vol. 510, Apr. 2020, doi: 10.1016/j.apsusc.2020.145492.

CERTIFICATE OF COMPLETENESS

It is hereby certified that the dissertation submitted by NS Muhammad Haseeb, Reg No. **00000277546**, Titled: ***Orthogonal Cutting of Gallium Nitride: A Numerical Investigation*** has been checked/reviewed and its contents are complete in all respects.

Supervisor's Name: **Dr. Hasan Aftab Saeed**   Signature: _____

                                                                                  Date: _____